

# **Subgingival calculus imaging based on swept-source optical coherence tomography**

Yao-Sheng Hsieh

Yi-Ching Ho

Shyh-Yuan Lee

Chih-Wei Lu

Cho-Pei Jiang

Ching-Cheng Chuang

Chun-Yang Wang

Chia-Wei Sun



# Subgingival calculus imaging based on swept-source optical coherence tomography

Yao-Sheng Hsieh,<sup>a,b</sup> Yi-Ching Ho,<sup>c</sup> Shyh-Yuan Lee,<sup>c,d</sup> Chih-Wei Lu,<sup>e</sup> Cho-Pei Jiang,<sup>f</sup> Ching-Cheng Chuang,<sup>g</sup> Chun-Yang Wang,<sup>b</sup> and Chia-Wei Sun<sup>a,b</sup>

<sup>a</sup>National Yang-Ming University, Biophotonics Interdisciplinary Research Center and Institute of Biophotonics, No. 155, Sec. 2, Linong Street, Taipei, Taiwan 112, Taipei, Taiwan

<sup>b</sup>National Chiao-Tung University, Department of Photonics, Hsinchu, Taiwan

<sup>c</sup>National Yang-Ming University, School of Dentistry, Taipei, Taiwan

<sup>d</sup>Taipei Veterans General Hospital, Department of Stomatology, Taipei, Taiwan

<sup>e</sup>Industrial Technology Research Institute, Medical Electronics and Device Technology Center, Hsinchu, Taiwan

<sup>f</sup>National Formosa University, Department of Power Mechanical Engineering, Yunlin, Taiwan

<sup>g</sup>National Taiwan University, Institute of Biomedical Engineering, Taipei, Taiwan

**Abstract.** We characterized and imaged dental calculus using swept-source optical coherence tomography (SS-OCT). The refractive indices of enamel, dentin, cementum, and calculus were measured as  $1.625 \pm 0.024$ ,  $1.534 \pm 0.029$ ,  $1.570 \pm 0.021$ , and  $2.097 \pm 0.094$ , respectively. Dental calculus leads strong scattering properties, and thus, the region can be identified from enamel with SS-OCT imaging. An extracted human tooth with calculus is covered with gingiva tissue as an *in vitro* sample for tomographic imaging. © 2011 Society of Photo-Optical Instrumentation Engineers (SPIE). [DOI: 10.1117/1.3602851]

Keywords: swept source optical coherence tomography; periodontitis; subgingival calculus.

Paper 10540SSRRR received Oct. 4, 2010; revised manuscript received May 20, 2011; accepted for publication Jun. 2, 2011; published online Jul. 25, 2011.

## 1 Introduction

Optical coherence tomography (OCT) was first reported by Fujimoto *et al.*<sup>1</sup> in 1991 and has been widely used in numerical clinical applications, including gastroenterology,<sup>2–4</sup> ophthalmology,<sup>5–7</sup> dermatology,<sup>8,9</sup> and dentistry.<sup>10,11</sup> In dental science, OCT can be an effective tool for assessing early caries,<sup>12–14</sup> oral cancer,<sup>15,16</sup> and periodontal diseases.<sup>17</sup> Periodontitis is one of the major chronic infectious diseases in the oral cavity, and the prevalence of periodontitis is >50% among the population.<sup>18,19</sup> The World Health Organization revealed that tooth loss resulting from severe periodontitis was found in 5–15% of most worldwide populations in 2003.<sup>20</sup> Additionally, recent studies have indicated that certain correlations between periodontitis and various systemic diseases exist.<sup>21–23</sup> Microbial dental plaque is an etiological factor of periodontitis, and dental calculus is a type of mineralized plaque from deposited microorganisms.<sup>24</sup> The traditional diagnosis of subgingival calculus is based on clinical examination using periodontal probing and radiographs. The poor reliability and reproducibility of periodontal probing causes monitoring the progression of periodontal destruction and the effects of treatments to be difficult.<sup>25–27</sup> Radiography can determine the level of bone-related destruction only for subgingival calculus located on the proximal surface of the teeth because of that x-rays cannot transmit hard tissues. The images of calculus on the buccal and lingual surfaces of a teeth are blocked; thus, it cannot be observed from radiography. In addition, the radiation exposure is accompanied by radiography measurement. Recently, several novel methods have

been developed for dental calculus detection, such as a smart ultrasonic device,<sup>17,28,29</sup> an LED-based optical probe,<sup>30</sup> and laser fluorescence.<sup>31,32</sup> Raman and laser fluorescence spectrometer may apply to calculus detection but are still under investigation. In fact, the Raman spectrometer is currently used for *in vitro* measurement. *In vivo* measurement is still applied today, but rarely. Laser fluorescence spectrometer should detect calculus using biotracer; however, the sensitivity and reliability are also poor.

Table 1 shows the comparison of general calculus detection methods used today. Compared to these methods, OCT may be an effective tool because it is a noninvasive, nondestructive, non-radiated, and real-time monitoring method. The swept-source optical coherence tomography (SS-OCT) has more benefits than conventional OCT. In this paper, we demonstrate the SS-OCT can be an effective tool for subgingival calculus detection in clinical diagnosis. The refractive indices of enamel, dentin, cementum, and dental calculus were measured for dental tissue characterization. The *in vitro* subgingival calculus was then imaged and processed for contrast improvement. The results show high-quality feasibility of dental calculus diagnosis based on SS-OCT.

## 2 Experiments and Results

### 2.1 Swept-Source Optical Coherence Tomography System

An SS-OCT system was built with a 1310-nm swept-source laser (Santec, HSL-2100) as a broadband light source. Figure 1(a) shows the picture of the SS-OCT setup, and Fig. 1(b) illustrates the system scheme. The fiber-based Mach-Zehnder

Address all correspondence to: Chia-Wei Sun, Biophotonics Interdisciplinary Research Center and Institute of Biophotonics, National Yang-Ming University, No. 155, Sec. 2, Linong Street, Taipei, Taiwan 112 Taiwan. Tel: 886228267028; Fax: 886228235460; E-mail: chiaweisun@ym.edu.tw

**Table 1** Comparison of calculus detection methods.

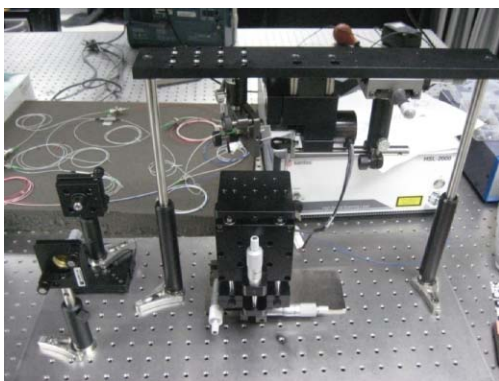
Methods	Advantages	Disadvantages
Radiography <sup>a</sup>	<ol style="list-style-type: none"> <li>1. Low cost</li> <li>2. Broad measurement range</li> </ol>	<ol style="list-style-type: none"> <li>1. Radiative</li> <li>2. Poor space resolution</li> <li>3. Calculus that locates on buccal and lingual surface of tooth will embed into tooth image</li> </ol>
Dental-CT <sup>a</sup>	<ol style="list-style-type: none"> <li>1. Broad measurement range</li> <li>2. 3-D image reconstruction is available</li> </ol>	<ol style="list-style-type: none"> <li>1. Expensive</li> <li>2. Real-time images are not available.</li> <li>3. Radiative</li> <li>4. Poor space resolution</li> </ol>
Intraoral Digital camera	<ol style="list-style-type: none"> <li>1. Low cost</li> <li>2. Convenient</li> <li>3. Nonradiative</li> </ol>	<ol style="list-style-type: none"> <li>1. Only surface information available</li> </ol>
Periodontal probe <sup>a</sup>	<ol style="list-style-type: none"> <li>1. Convenient</li> <li>2. Low cost</li> <li>3. Broad measurement range</li> </ol>	<ol style="list-style-type: none"> <li>1. Low sensitivity</li> <li>2. No images</li> <li>3. Invasive</li> <li>4. Uncomfortable</li> </ol>
Sirona PerioScan (piezoelectric device) <sup>b</sup>	<ol style="list-style-type: none"> <li>1. Detection of subgingival calculus during ultrasonic scaling</li> </ol>	<ol style="list-style-type: none"> <li>1. Invasive, uncomfortable</li> <li>2. Learning curve required</li> </ol>
OCT	<ol style="list-style-type: none"> <li>1. High space resolution</li> <li>2. Real-time images to differentiate dental structure</li> <li>3. Nonradiative oral probe was developed</li> <li>4. 3-D image reconstruction is available</li> </ol>	<ol style="list-style-type: none"> <li>1. Limited penetration depth</li> </ol>
SS-OCT <sup>c-e</sup> (compare to other OCT)	<ol style="list-style-type: none"> <li>1. Higher imaging speed</li> <li>2. Higher detection efficiency</li> <li>3. Higher sensitivity</li> <li>4. Simpler</li> <li>5. Better SNR with suitable filter</li> </ol>	<ol style="list-style-type: none"> <li>1. Expensive</li> <li>2. Very high speed data acquisition interface is necessary</li> </ol>
Raman spectroscopy <sup>f-h</sup>	<ol style="list-style-type: none"> <li>1. High sensitivity</li> <li>2. Simple sample preparation</li> <li>3. Easy spectral analysis</li> <li>4. Responses to mineral and chemical concentrations are available</li> </ol>	<ol style="list-style-type: none"> <li>1. <i>In vitro</i> experiment only</li> <li>2. Expensive</li> <li>3. No images</li> </ol>
Laser fluorescence spectrometer <sup>f,i</sup>	<ol style="list-style-type: none"> <li>1. Real time detection</li> <li>2. Responses to bacteria and chemical concentrations are available</li> <li>3. Easy spectral analysis</li> </ol>	<ol style="list-style-type: none"> <li>1. <i>In vitro</i> experiment</li> <li>2. No images</li> </ol>

<sup>a</sup>Reference 17.<sup>b</sup>Reference 33.<sup>c</sup>Reference 34.<sup>d</sup>Reference 35.<sup>e</sup>Reference 36.<sup>f</sup>Reference 37.<sup>g</sup>Reference 38.<sup>h</sup>Reference 39.<sup>i</sup>Reference 31.<sup>j</sup>Reference 32.

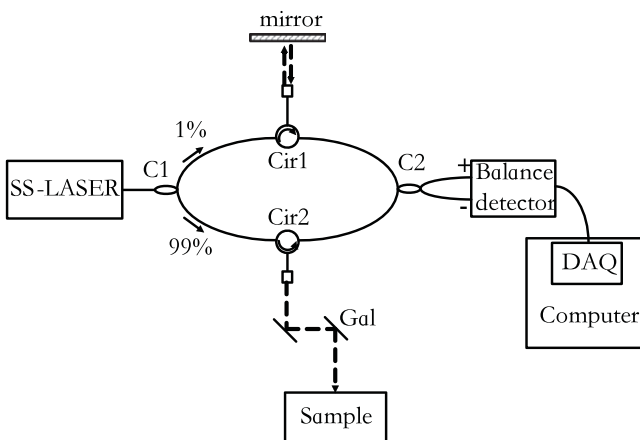
interferometer was adopted with two couplers (one is 99:1, and the other is 50:50), and two optical circulators. The illumination power of the sample arm was 0.8 mW, and the power of the reference arm was 0.6  $\mu$ W. The balance detector was utilized for interference detection, and the data acquisition card (DAQ card, NI-PCI 5122) was then used for computer-photodetector interfacing. In our *in vitro* study, all samples were placed on a three-dimensional translation stage for optical scanning. The wavelength-scanning rate is 20 kHz. The frame rate is 20 Hz (1000 A-scans/frame). The electric signals acquisition rate is 100 MS/s by NI-PCI 5122. Experimental data were collected and analyzed using LabVIEW (National Instrument) software. Dispersion compensation and interpolation were also completed using LabVIEW. We saved the OCT images per 100  $\mu$ m length. Because of the width of the tooth being  $\sim$ 1.2 cm, around 120 images were observed. For imaging the whole tooth, 200 images were taken in the experiments.

### 2.2 Refractive Indices Measurement

The refractive index determines the optical property of material. In previous studies,<sup>40,41</sup> the refractive index of a highly scattering sample could be estimated from OCT measurement (as



(a)



(b)

**Fig. 1** (a) Inrange of SS-OCT system and (b) schematic diagram of SS-OCT system. C1: 99:1 fiber coupler; C2: 50:50 fiber coupler; Cir1, Cir2: optical circulators; Gal: galvanometer.

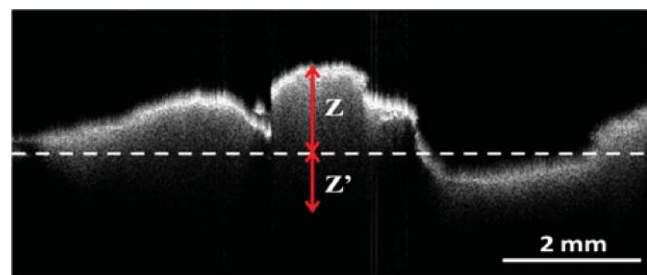
**Table 2** Refractive indices of dental tissues and glass slide.

	Refractive index
Enamel	$1.619 \pm 0.034$
Dentin	$1.528 \pm 0.026$
Cementum	$1.567 \pm 0.030$
Calculus	$2.112 \pm 0.127$
Glass slide	$1.503 \pm 0.018$

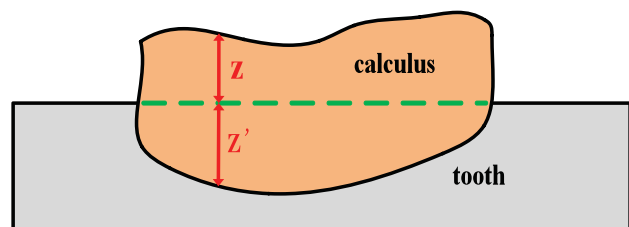
shown in Fig. 2). The lengths of the upper and lower parts are defined as  $z$  and  $z'$  and the refractive index is

$$n = 1 + \frac{z'}{z}$$

The refractive indices of enamel, dentin, and cementum were calculated following the method of Ref. 40. For calculating the refractive index of calculus, some clear definition of boundaries of  $z$  and  $z'$  should be discussed because the lower boundary of  $z'$  should choose a line that light can pass through as easily as possible. We chose three boundary lines in the OCT image for defining the boundary of refractive index calculation. The upper line is the top of the calculus. The middle line is the extension of the tooth surface from the left side to the right side of the calculus. The bottom line is the line that passes through the lower boundary of the calculus. Therefore, the chosen line that locates the bottom of the enamel instead of the bottom of the calculus is not easy to define in the real margin. Figure 3 shows the OCT images of glass, enamel, dentin, and cementum samples. Each sample was polished as a thin slice for



(a)



(b)

**Fig. 2** (a) SS-OCT image of dental calculus and (b) scheme of dental calculus.

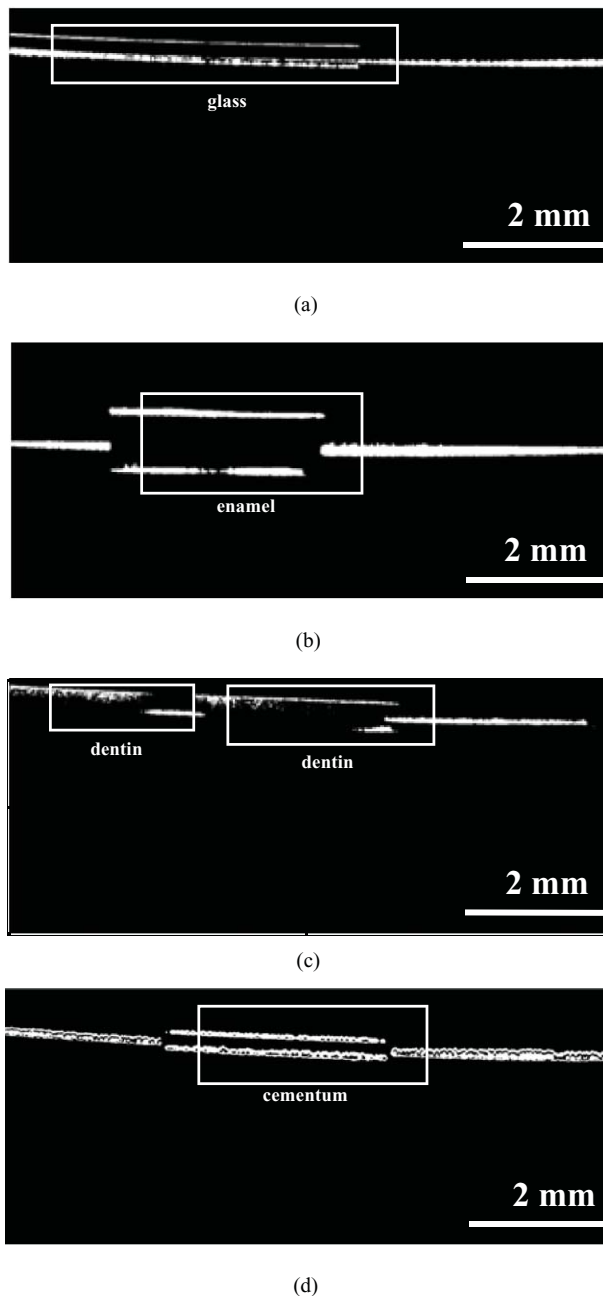


**Fig. 3** SS-OCT images of (a) glass, (b) enamel, (c) dentin, and (d) cementum.

SS-OCT measurement. All the OCT images were processed with a Gaussian filter and then binarized for contrast improvement. A (2×6)-mm glass slide was used as a standard sample for refractive index measurements calibration because its refractive index is well known. To avoid multireflection, the glass slide was placed on a (3×8)-mm rough-surfaced aluminum bar. Figure 3(a) is the OCT image of the glass slide. To observe the refractive index, we chose 20 points for each sample and five samples were measured in the OCT image of the glass slide for calculation. The refractive index of the glass slide is  $1.503 \pm 0.018$  and extremely close to the typical glass refractive index of 1.52.<sup>42</sup> Table 2 lists the refractive indices of enamel, dentin, cementum, calculus, and the glass slide, which were each measured as  $1.625 \pm 0.024$ ,  $1.534 \pm 0.029$ ,  $1.570 \pm 0.02$ ,

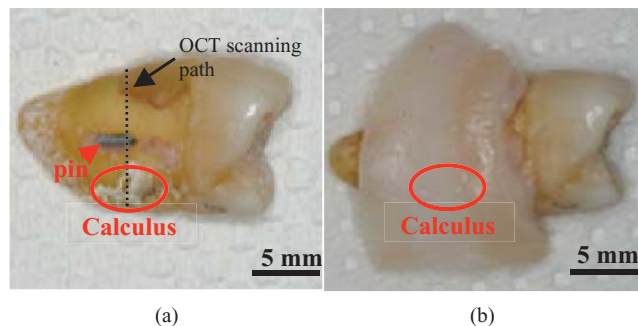
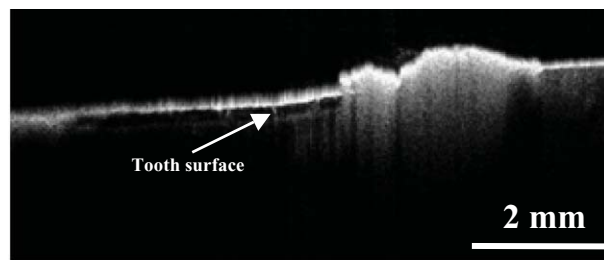


**Fig. 4** (a) Dental calculus sample and (b) gingival tissue covered on the sample of dental calculus.

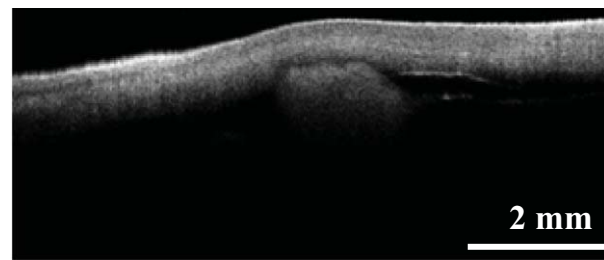
$2.097 \pm 0.094$ , and  $1.503 \pm 0.018$ , respectively. These measurements strongly agree with previous results.<sup>41</sup>

### 2.3 In Vitro Dental Calculus Imaging

Figure 4 demonstrates the *in vitro* sample of dental calculus. One human caries-free tooth with subgingival calculus, extracted for periodontal reasons, was enrolled. The calculus region was marked on the surface of the tooth. For feasible study of subgingival calculus detection, a piece of porcine gingiva tissue with 0.8-mm thickness was used to cover the tooth sample. For effective position alignment, the tooth was fixed on beeswax and attached to a platform before applying gingiva to the tooth. Furthermore, an iron pin was placed on the surface next to the calculus to ensure the same measurement location because the iron pin shows an obviously high reflection property in the OCT image. The measurement path that passes through the pin for alignment subject is shown in Fig. 4. We moved the platform at 100  $\mu\text{m}$  between images; hence, measuring at the same location was possible if the platform moved in a reverse direction at the

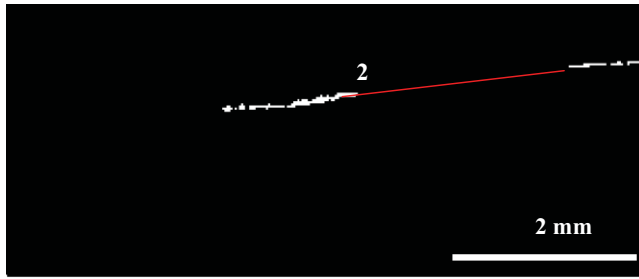


(a)

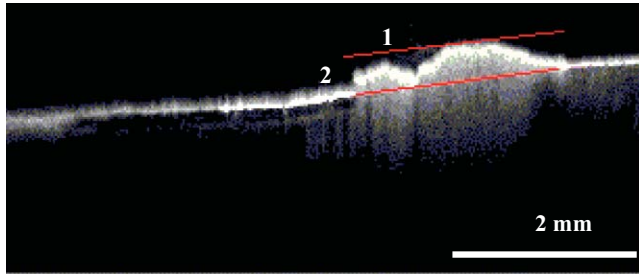


(b)

**Fig. 5** (a) OCT image of dental calculus and (b) OCT image of subgingival calculus.



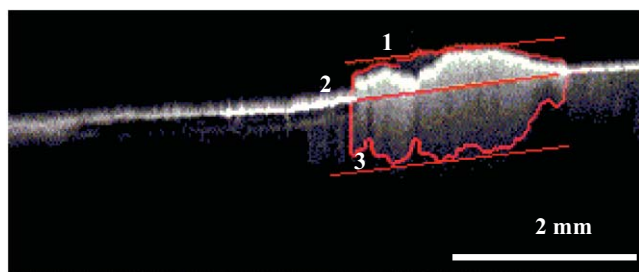
(a)



(b)



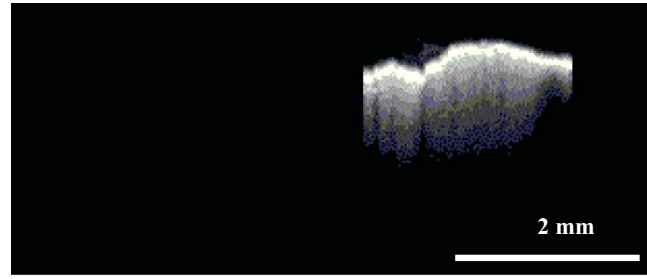
(c)



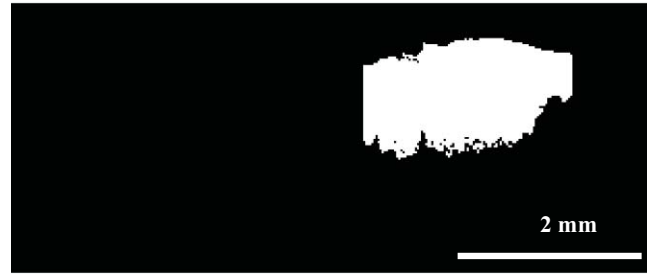
(d)

**Fig. 6** Image process for lines decision: (a) Removing the calculus and keeping the tooth surface for second line drawing, (b) the first line drawing, (c) the margin detection of calculus, and (d) the third line drawing and boundaries of refractive index calculation.

same distance after applying gingiva to the tooth. Therefore, images with the same number show a favorable comparison. We also controlled where the pin image is displayed in OCT images to ensure that the entire experiment began at the same location and that the OCT calculus images allowed for an effective comparison. Figure 5 shows the OCT images of the sample with respect to Fig. 4. By scanning along the path (the dotted line in Fig. 4), the OCT images of normal tooth surface and calculus can be observed in Fig. 5. Figure 5(a) shows the calculus region that corresponds to Fig. 4(a), and Fig. 5(b) demonstrates the



(a)



(b)



(c)



(d)

**Fig. 7** The calculus region with threshold filtering: (a) original image, (b) 0.01 threshold value processing, (c) 0.3 threshold value processing, and (d) 0.18 threshold value processing.

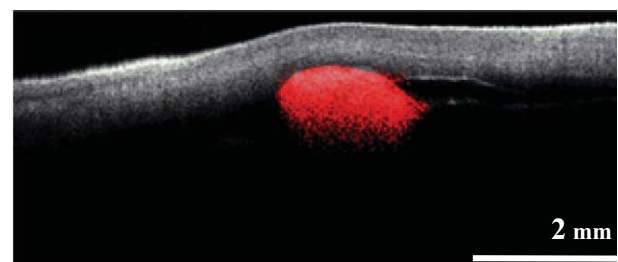


**Fig. 8** Postprocessed subgingival calculus image.

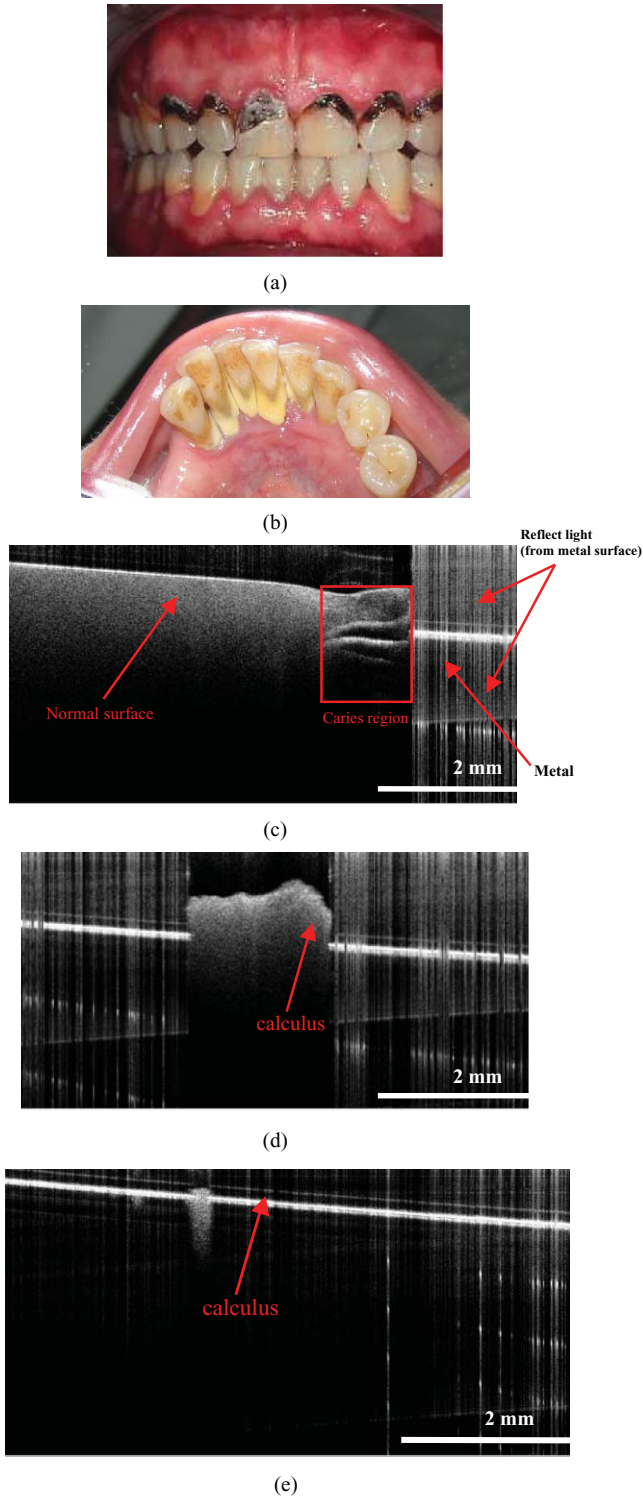


**Fig. 9** (a) Images of caries and (b) calculus deposition on lingual side of mandibular incisors. (c) OCT image of caries, (d) OCT image of calculus, and (e) OCT image of grinded calculus.

subgingival calculus image that corresponds to Fig. 4(b). Although the gingival layer attenuates the optical signal, the calculus region can also be seen in Fig. 5(b).

Before the determination of refractive index, three boundary lines should be given. The measured image was postprocessed

with an anisotropic diffusion filter, midvalue filter, and threshold filter for noise suppression and identified the position of calculus edge.<sup>43</sup> These processes were also used for determining the boundary lines. Because of the surface of teeth can be observed directly from the OCT image, the second line was decided first. In Fig. 6(a), we had removed other parts except teeth surface and approach the second line. The threshold filter and Gaussian filter were used to remove the calculus and keep the tooth surface. As shown in Fig. 6(a), we kept tooth surface and connected two ends of the surface as the second line. The first line was decided as a parallel to second line and pass through the top point of calculus [Fig. 6(b)]. Next, the edge filter was used to obtain the calculus margin. In Fig. 6(c), we found the lowest point of calculus margin and decided the third line passes through the point with parallel to the other lines. This approach provides an easy way to estimate the refractive index for dental tissue characterizing. The boundaries of  $z$  and  $z'$  are indicated in Fig. 6(d).

For optimization of image process, we separated calculus image with threshold and Gaussian filters. Figure 7 shows the processed images with different threshold values. Obviously, the processed calculus size depends on the threshold value in the gray-scale threshold filter. We chose the threshold value trial and error for imaging optimization.<sup>44-46</sup> The optimal threshold value is 0.18. Because the parameters of OCT operation and image process are set as the optimal values, the errors of linear approximation can then be reduced. In clinical diagnoses, the OCT image provides great assistance if the dental calculus region can be highlighted accurately. The dental calculus region can be featured after this processing. Figure 8 shows the processed subgingival calculus image, and the calculus region is marked in red.

### 3 Discussion and Conclusion

Although many studies have reported that caries detection could be achieved based on OCT imaging, we demonstrate a method that can be applied to subgingival calculus detection in dentistry. Moreover, the refractive index of dental calculus was measured in experiment. The dental calculus shows different optical and image properties to the caries. In Fig. 9, we can find that the dental calculus shows different optical and image properties to the caries. The caries reveal lower group delay and destroy the tooth structure inwardly. On the other hand, the calculus shows stronger group delay and do not affect the tooth structure because the calculus always deposits on the tooth surface. The different features can be observed in OCT images. Figure 9(e) shows the small volume of calculus still reveals the same property of strong group delay. Therefore, the difference between caries and calculus can be diagnosed by direct OCT imaging. In clinical diagnoses, the method presents advantages when compared to conventional x-ray imaging. X-ray imaging is radioactive and cannot observe the calculus on the buccal or lingual surface of the tooth. However, OCT imaging can overcome these two drawbacks. For further study, an oral probe will be developed instead of the sample arm for *in vivo* measurement.

A linear boundary approximation method was used in this paper for refractive index calculation. This method provides an estimation of refractive index fast and easy. Errors of linear approximation occur with rough surface and nonlinear boundary

of dental tissue. However, it should be sufficient for understanding the characterizations of teeth and calculus in our experiment.

We demonstrated the subgingival calculus detection method using SS-OCT at 1310 nm with a Mach-Zehnder interferometer. The refractive indices of tooth tissue as enamel, dentin, cementum, and calculus were  $1.625 \pm 0.024$ ,  $1.534 \pm 0.029$ ,  $1.570 \pm 0.021$ , and  $2.097 \pm 0.094$ , respectively. Calculus revealed a strong scattering property that originated with a high refractive index. For subgingival calculus imaging, a human tooth with 0.8 mm porcine gingiva was employed as an *in vitro* sample in the experiment. The dental calculus region could then be marked with the postprocess. The experimental results indicate that the SS-OCT can be of great assistance for dental calculus detection. Currently, the handheld probe is under development for further *in vivo* study.

### Acknowledgments

This work was supported by the National Science Council of Taiwan under Grants No. NSC 99-2221-E-010-011, No. NSC 99-2622-E-010-001-CC3, and No. NSC 98-2221-E-010-004.

### References

- D. Huang, E. A. Swanson, C. P. Lin, J. S. Schuman, W. G. Stinson, W. Chang, M. R. Hee, T. Flotte, K. Gregory, C. A. Puliafito, and J. G. Fujimoto, "Optical coherence tomography," *Science* **254**(5035), 1178–1181 (1991).
- J. M. Ponomarev, S. Brand, B. E. Bouma, G. J. Tearney, C. C. Compton, and N. S. Nishioka, "Diagnosis of specialized intestinal metaplasia by optical coherence tomography," *Gastroenterology* **120**(1), 7–12 (2001).
- J. A. Evans, J. M. Ponomarev, B. E. Bouma, J. Bressner, E. F. Halpern, M. Shishkov, G. Y. Lauwers, M. M. Kenudson, N. S. Nishioka, and G. J. Tearney, "Optical coherence tomography to identify intramucosal carcinoma and high-grade dysplasia in Barrett's esophagus," *Clin. Gastroenterol. Hepatol.* **4**(1), 38–43 (2006).
- P. W. Smith, K. Lee, S. Guo, J. Zhang, K. Osann, Z. Chen, and D. Messadi, "In Vivo Diagnosis of Oral Dysplasia and Malignancy Using Optical Coherence Tomography: Preliminary Studies in 50 Patients," *Lasers Surg. Med.* **41**(5), 353–357 (2009).
- Y. Wang, B. A. Bower, J. A. Izatt, O. Tan, and D. Huang, "Retinal blood flow measurement by circumpapillary Fourier domain Doppler optical coherence tomography," *J. Biomed. Opt.* **13**(6), 064003 (2008).
- M. Hangai, Y. Ojima, N. Gotoh, R. Inoue, Y. Yasuno, S. Makita, M. Yamanari, T. Yatagai, M. Kita, and N. Yoshimura, "Three-dimensional imaging of macular holes with high-speed optical coherence tomography," *Ophthalmology* **114**(4), 763–773 (2007).
- Y. Yasuno, Y. Hong, S. Makita, M. Yamanari, M. Akiba, M. Miura, and T. Yatagai, "In vivo high-contrast imaging of deep posterior eye by 1- $\mu$ m swept source optical coherence tomography and scattering optical coherence angiography," *Opt. Express* **15**(10), 6121–6139 (2007).
- A. Pagnoni, A. Knuettel, P. Welker, M. Rist, T. Stoudemayer, L. Kolbe, I. Sadiq, and A. M. Kligman, "Optical coherence tomography in dermatology," *Skin Res. Technol.* **5**(2), 83–87 (1999).
- M. C. Pierce, J. Strasswimmer, B. H. Park, B. Cense, and J. F. de Boer, "Birefringence measurements in human skin using polarization-sensitive optical coherence tomography," *J. Biomed. Opt.* **9**(2), 287–291 (2004).
- B. W. Colston, Jr., U. S. Sathyam, L. B. DaSilva, M. J. Everett, P. Stroeve, and L. L. Otis, "Dental OCT," *Opt. Express* **3**(6), 230–238 (1998).
- A. Baumgartner, S. Dichtl, C. K. Hitzberger, H. Sattmann, B. Robl, A. Moritz, A. F. Fercher, and W. Sperr, "Polarization-sensitive optical coherence tomography of dental structures," *Caries Res.* **34**(1), 59–69 (2000).
- D. Fried, J. Xie, S. Shafi, J. D. B. Featherstone, T. M. Breunig, and C. Le, "Imaging caries lesions and lesion progression with polarization sensitive optical coherence tomography," *J. Biomed. Opt.* **7**(4), 618–627 (2002).
- B. T. Amaechi, S. M. Higham, A. G. Podoleanu, J. A. Rogers, and D. A. Jackson, "Use of optical coherence tomography for assessment of dental caries: quantitative procedure," *J. Oral Rehab.* **28**(12), 1092–1093 (2001).
- B. T. Amaechi, A. Podoleanu, S. M. Higham, and D. A. Jackson, "Correlation of quantitative light-induced fluorescence and optical coherence tomography applied for detection and quantification of early dental caries," *J. Biomed. Opt.* **8**(4), 642–647 (2003).
- P. W. Smith, W. G. Jung, M. B. K. Osann, H. Beydoun, D. Messadi, and Z. Chen, "In vivo optical coherence tomography for the diagnosis of oral malignancy," *Lasers Surg. Med.* **35**(4), 269–275 (2004).
- C. C. Yang, M. T. Tsai, H. C. Lee, C. K. Lee, C. H. Yu, H. M. Chen, C. P. Chiang, C. C. Chang, Y. M. Wang, and C. C. Yang, "Effective indicators for diagnosis of oral cancer using optical coherence tomography," *Opt. Express* **16**(20), 15847–15862 (2008).
- X. Xiang, M. G. Sowa, A. M. Iacopino, R. G. Maev, M. D. Hewko, A. Man, and K. Z. Liu, "An update on novel non-invasive approaches for periodontal diagnosis," *J. Periodontol.* **81**(2), 186–198 (2009).
- A. Hugoson, B. Sjödin, and O. Norderyd, "Trends over 30 years, 1973–2003, in the prevalence and severity of periodontal disease," *J. Clin. Periodontol.* **35**(5), 405–414 (2008).
- L. J. Brown and H. Loe, "Prevalence, extent, severity and progression of periodontal disease," *Periodontol.* **2000** **2**(1), 57–71 (1993).
- P. E. Petersen, *The World Oral Health Report*, World Health Organization, Geneva, Switzerland (2003).
- Y. S. Khader and Q. Ta'ani, "Periodontal diseases and the risk of preterm birth and low birth weight: a meta-analysis," *J. Periodontol.* **76**(2), 161–165 (2005).
- J. D. Beck and S. Offenbach, "Systemic effects of periodontitis: epidemiology of periodontal disease and cardiovascular disease," *J. Periodontol.* **76**(11-s), 2089–2100 (2005).
- A. M. Iacopino and C. W. Cutler, "Pathophysiological relationships between periodontitis and systemic disease: recent concepts involving serum lipids," *J. Periodontol.* **71**(8), 1375–1384 (2000).
- E. A. R. Harry and V. Clerehugh, "Subgingival calculus: where are we now? a comparative review," *J. Dent.* **28**(2), 93–102 (2000).
- D. M. Aeppli, J. R. Boen, and C. L. Bandt, "Measuring and interpreting increases in probing depth and attachment loss," *J. Periodontol.* **56**(5), 262–264 (1985).
- A. Badersten, R. Nilvéus, and J. Egelberg, "Reproducibility of probing attachment level measurements," *J. Clin. Periodontol.* **11**(7), 475–485 (1984).
- J. M. Goodson, A. C. Tanner, A. D. Haffajee, G. C. Sornberger, and S. S. Socransky, "Patterns of progression and regression of advanced destructive periodontal disease," *J. Clin. Periodontol.* **9**(6), 472–481 (1982).
- G. Meissner, B. Oehme, J. Strackeljan, and T. Kocher, "Clinical subgingival calculus detection with a smart ultrasonic device: a pilot study," *J. Clin. Periodontol.* **35**(2), 126–132 (2008).
- G. Meissner, B. Oehme, J. Strackeljan, and T. Kocher, "A new system to detect residual subgingival calculus: *in vitro* detection limits," *J. Clin. Periodontol.* **33**(3), 195–199 (2006).
- F. Krause, A. Braun, S. Jepsen, and M. Frenzen, "Detection of subgingival calculus with a novel LED-based optical probe," *J. Periodontol.* **76**(7), 1202–1206 (2005).
- E. Kurihara, T. Koseki, K. Gohara, T. Nishihara, T. Ansai, and T. Takehara, "Detection of subgingival calculus and dentine caries by laser fluorescence," *J. Periodont. Res.* **39**(1), 59–65 (2004).
- M. Folwaczny, R. Heym, A. Mehl, and R. Hickel, "Subgingival calculus detection with fluorescence induced by 655 nm InGaAsP diode laser radiation," *J. Periodontol.* **73**(6), 597–601 (2002).
- L. J. Walsh, "Exploiting sound and the piezoelectric effect for real time calculus detection: PerioScan and the transducer concept," *Australas. Dent. Practice* **19**(3), 54–58 (2008).
- M. A. Choma, M. V. Sarunic, C. Yang, and J. A. Izatt, "Sensitivity advantage of swept source and Fourier domain optical coherence tomography," *Opt. Express* **11**(18), 2183–2189 (2003).
- V. J. Srinivasan, R. Huber, I. Gorczynska, J. Y. Jiang, P. Reisen, A. E. Cable, and J. G. Fujimoto, "High-speed, high-resolution

- optical coherence tomography retinal imaging with a frequency-swept laser at 850 nm," *Opt. Lett.* **32**(4), 361–363 (2007).
36. B. Liu and M. E. Brezinski, "Theoretical and practical considerations on detection performance of time domain, Fourier domain, and swept source optical coherence tomography," *J. Biomed. Opt.* **12**(4), 044007 (2007).
  37. H. Tsuda and J. Arends, "Raman spectroscopy in human dental calculus," *J. Dental Res.*, **72**(12), 1609–1613 (1993).
  38. P. Carmona, J. Bellanato, E. Escobar, "Infrared and Raman spectroscopy of urinary calculi: A review," *Biospectroscopy* **3**(5), 331–346 (1997).
  39. H. Tsuda and J. Arends, "Raman spectroscopy in dental research: a short review of recent studies," *J. Dent. Res.* **11**(4), 539–547 (1997).
  40. G. J. Tearney, M. E. Brezinski, J. F. Southern, B. E. Bouma, M. R. Hee, and J. G. Fujimoto, "Determination of the refractive index of highly scattering human tissue by optical coherence tomography," *Opt. Lett.* **20**(21), 2258–2260 (1995).
  41. Z. Meng, X. S. Yao, H. Yao, Y. Liang, T. Liu, Y. Li, G. Wang, and S. Lan, "Measurement of the refractive index of human teeth by optical coherence tomography," *J. Biomed. Opt.* **14**(3), 034010 (2009).
  42. F. L. Pedrotti, L. S. Pedrotti, and L. M. Pedrotti, *Introduction to Optics*, 3th ed., pp. 455, Pearson Education, Inc., Upper Saddle River, New Jersey (2007).
  43. M. H. Le, C. L. Darling, and D. Fried, "Automated analysis of lesion depth and integrated reflectivity in PS-OCT scan of tooth demineralization," *Lasers Surg. Med.* **42**(1), 62–68 (2010).
  44. N. Otsu, "A threshold selection method from gray-level histograms," *IEEE Trans. Syst. Man. Cybernet.* **9**(1), 62–66 (1979).
  45. H. Zhang, J. E. Fritts, and S. A. Goldman, "Image segmentation evaluation: a survey of unsupervised methods," *Comput. Vis. Image Understand.* **110**(2), 260–280 (May 2008).
  46. M. Sezgin and B. Sankur, "Survey over image thresholding techniques and quantitative performance evaluation," *J. Electron. Imaging.* **13**(1), 146–165 (2004).